Evaluation of indole-based organometallics as transfer hydrogenation catalysts with anticancer activity

Laia Rafols, Maria Azmanova, Nathan Perrigault, Patricia Cooper, Steven Shnyder, William H.C. Martin, Anaïs Pitto-Barry

Journal of Organometallic Chemistry 1013 (2024) 123168

Contents lists available at ScienceDirect

Journal of Organometallic Chemistry

journal homepage: www.elsevier.com/locate/jorganchem

Evaluation of indole-based organometallics as transfer hydrogenation catalysts with anticancer activity☆

Laia Rafols [a], Maria Azmanova [a,b], Nathan Perrigault [c], Patricia A. Cooper [b], Steven D. Shnyder [b], William H.C. Martin [a], Anaïs Pitto-Barry [c,*]

[a] School of Chemistry and Biosciences, University of Bradford, Bradford, BD7 1DP, United Kingdom
[b] School of Pharmacy and Medical Sciences, University of Bradford, Bradford, BD7 1DP, United Kingdom
[c] Université Paris-Saclay, CNRS, Institut Galien Paris-Saclay, 91400 Orsay, France

ARTICLE INFO

Keywords:
Bioorganometallic chemistry
Metal-based drugs
Bioactive ligand
Catalysis in cells

ABSTRACT

Half-sandwich complexes containing transition metals offer a wide range of applications owing to their interactions with a variety of targets/molecules that are not accessible for some organic scaffolds. The use of such complexes is therefore a way to provide new mechanisms of drug action. Here, we report a series of neutral metal complexes of the type [(arene)M(O-cyclohexyl-1*H*-indole-2-carbothiolate)Cl] that have the ability to reduce the coenzyme NAD^+ at physiological conditions in the presence of sodium formate as an hydride donor. The influence of the metal ion (Ru, Os, Rh, Ir) is studied to establish some structure-activity relationships. The [(η^6-*p*-cym)Ru(O-cyclohexyl-*1H*-indole-2-carbothioate)Cl] is the most active catalyst of this family of complexes with a turnover frequency (TOF) of 14.79 h^{-1} for the transfer hydrogenation reaction of NAD^+ to give 1,4-NADH in the presence of formate. Further *in vitro* studies were carried out to determine a relationship between catalytic activity and potency as an anticancer drug, with the rhodium complex promisingly showing 7x more selectivity towards cancer cells (A2780) than normal cells (PNT2). Preliminary *in vivo* studies demonstrated the importance of co-treatment with formate to enhance activity. This work gives insights into the mechanism of action of this family of indole-based organometallic complexes.

1. Introduction

Cancer is a set of diseases with a significant worldwide impact and is the second cause of death globally (1 in 6 deaths in 2018) [1]. One of the most used treatments for this set of diseases is cisplatin, a coordination compound based on platinum [2,3] Despite their success, cisplatin and its derivatives produce severe side effects, pointing out the urgent need to discover more effective and less harmful anticancer agents [4–8].

In the field of bioinorganic chemistry, ruthenium stands out as an attractive alternative to platinum-based drugs with two compounds currently undergoing clinical trials, BOLD-100 and TLD-1433 (Fig. 1) [9,10]. Organometallic compounds containing ruthenium have also been exploited for their efficiency as catalysts in many organic transformations, both in a round-bottom flask, such as cross-metathesis [11,12], and in cells [13–17]. Transition metal catalysts have potential as therapeutic agents as they are able to transform multiple substrate molecules whilst requiring low concentrations to achieve the desired activity. More recently, Sadler et al. developed a series of compounds based on a Ru(II) Noyori-type catalyst capable of producing transfer hydrogenation reactions within living organisms, prompting the use of these catalytic drugs as an alternative therapy [15,18,19]. This family of complexes containing a sulfonamidoethylenediamine-chelated ligand was able to reduce NAD^+ to NADH in presence of an hydride donor under physiological conditions. It was discovered that changes in the sulfonamide ligand could modify the turnover frequencies of these compounds. The bulkier the group was, the more the catalytic activity of the compound was enhanced, with the best candidate being the complex containing a benzyl group in the tosylethylenediamine ligand [20–22]. This discovery encouraged the exploration of this type of complexes that showed a great potential of activity at lower dosages, as well as introducing new mechanisms of action to overcome side effects observed for platinum complexes [23–25].

We have recently reported a series of half-sandwich ruthenium(II) complexes containing an indole-based chelated ligand with promising

☆ Dedicated to Prof. Nicolas Pierre Edouard Barry who passed away on the 16th of March 2023

* Corresponding author.
E-mail address: anais.pitto-barry@universite-paris-saclay.fr (A. Pitto-Barry).

https://doi.org/10.1016/j.jorganchem.2024.123168
Received 14 January 2024; Received in revised form 30 April 2024; Accepted 2 May 2024
Available online 6 May 2024

antibacterial activity, with [(*p*-cym)Ru(O-cyclohexyl-*1H*-indole-2-carbothioate)Cl] (compound **1** in Fig. 1) being the most active complex against a broad spectrum of antibiotic-resistant bacteria such as *Mycobacterium tuberculosis* and *Salmonella enterica* [26]. Besides these promising results, this ruthenium(II) complex showed an interesting turnover rate as a transfer hydrogenation catalyst for the reaction of the cofactors NAD^+/NADH. Based on this discovery and in order to establish in-depth structure-activity relationships (SARs), we decided to investigate the influence of the metal ion for complexes containing the ligand [cyclohexyl indole-2-thionoester].

Herein, we report the synthesis and characterisation of four new half-sandwich complexes with the general formula [(arene)M(O-cyclohexyl-*1H*-indole-2-carbothioate)Cl], namely [(*p*-cym)Ru(O-cyclohexyl-*1H*-indole-2-carbothioate)Cl] (**1**), [(*p*-cym)Os(O-cyclohexyl-*1H*-indole-2-carbothioate)Cl] (**2**), [Cp*-Rh(O-cyclohexyl-*1H*-indole-2-carbothioate)Cl] (**3**) and [Cp*-Ir(O-cyclohexyl-*1H*-indole-2-carbothioate)Cl] (**4**) (Fig. 2). The ability of these complexes to alter the NAD^+/NADH ratio is studied by NMR and UV–Vis spectroscopies. Additionally, the antiproliferative activity against two ovarian cancer (A2780 and A2780cisR) and normal prostate (PNT2) cell lines is described. To correlate the catalytic activity of these complexes in test tubes and in cells, co-incubation studies with sodium formate and *N*-acetylcysteine (NAC) are reported for all organometallic complexes. Over the past ten years, there has been an increasing interest in utilising organometallic complexes as biocatalysts to replicate the exceptional selectivity and efficiency of metalloenzymes present in the human body [27–30]. However, there are currently no reported compounds that contain indole-based ligands with the capability of producing transfer hydrogenation catalysis in living organisms [20,23,31]. While the possibility of using such complexes *in vivo* seems promising, there is really scarce data on catalytic studies on mice, as this possible mechanism of action is still unclear. For this reason, and based on the *in vitro* results, complex **1** was selected for progression *in vivo*, as it presented the best catalytic activity of the four complexes *in vitro*. Complex **1** was therefore administered alone and in combination with formate in mice bearing A2780 and A2780cisR tumours. This study demonstrated that high dosages of sodium formate can be tolerated by living organisms, and that led to an improvement of the cytotoxic activity of **1** against these two subcutaneous tumour xenograft models.

2. Results and discussion

2.1. Synthesis, stability in solution, aquation, pKa, and Log P determination

The syntheses of the ligand O—Cy—*1H*—indole-2-carbothiolate and the complex [(*p*-cym)Ru(O—Cy—ind—th)Cl] (**1**) were previously reported by our group in 2022 for antibacterial purposes [26]. Briefly, the ligand was prepared in two steps, by esterification of 1H-indole-2-carboxylic acid with cyclohexanol followed by thiolation with Lawesson's reagent. Osmium, rhodium, and iridium have been chosen to better understand the role played by the metal centre in the biological activity of such an architecture as it has been shown that moving from group 8 to group 9 or from period 5 to period 6 can have a tremendous effect on their structure-activity relationships (Scheme 1) [32].

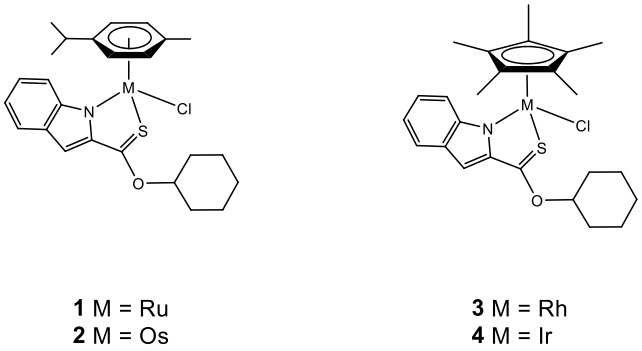

Fig. 2. Chemical structures of the piano-stool complexes **1** – **4**.

Herein, the syntheses and characterisation of three new complexes based on the O—Cy-*1H*-indole-2-carbothiolate ligand, namely, [(*p*-cym)Os(O-cyclohexyl-*1H*-indole-2-carbothioate)Cl] (**2**), [Cp*-Rh(O-cyclohexyl-*1H*-indole-2-carbothioate)Cl] (**3**) and [Cp*-Ir(O-cyclohexyl-*1H*-indole-2-carbothioate)Cl] (**4**) are described. All complexes were prepared by stirring the respective dichloro(arene)metal dimer with the cyclohexyl ligand in dry dichloromethane at ambient temperature and in the presence of triethylamine, to accelerate the splitting of the metal dimer upon coordination to the indole-based ligand [27]. Complexes **2** – **4** were characterised by ^1H and ^{13}C NMR spectroscopies (see Figs. 3 and S1-S6), and high-resolution mass spectrometry (ESI-MS) (see Figures S7-S10).

Owing to differences in their stabilities in solution, complexes **1** – **3** were dissolved in $CDCl_3$ while complex **4** was dissolved in CD_2Cl_2, which is likely to be explained by the residual acidity of $CDCl_3$. All NMR spectra of the complexes showed the expected significant peaks. The aromatic protons of the lowest field region (9.5 – 7 ppm) confirm the coordination of the indole-based substituent, whilst the coordinated arene protons of complex **1** and **2** and the CH proton of the cyclohexyl group are visible in the range 6.5 – 5 ppm. Finally, the aliphatic region (3 – 0.5 ppm) shows the rest of the cyclohexyl group and the methyl groups of the arene for complexes **1** - **4**. The signal for the NH proton is no more visible after complexation whilst the proton of the CH cyclohexyl bonded to the heteroatom O is shifted upfield after the coordination takes place, as expected owing to stereo-electronic effects [33]. These spectra demonstrate the successful coordination of the indole-based moiety to the metal centre for all complexes.

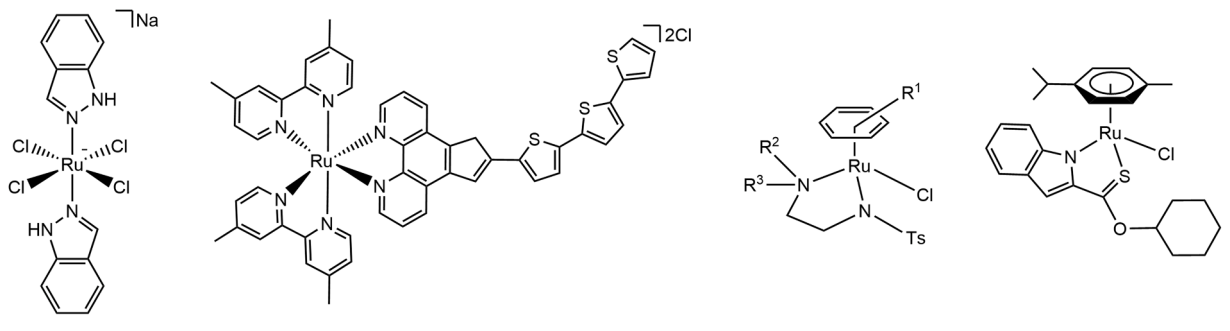

Fig. 1. Chemical structures of the most relevant ruthenium-based anticancer compounds and complex **1**.

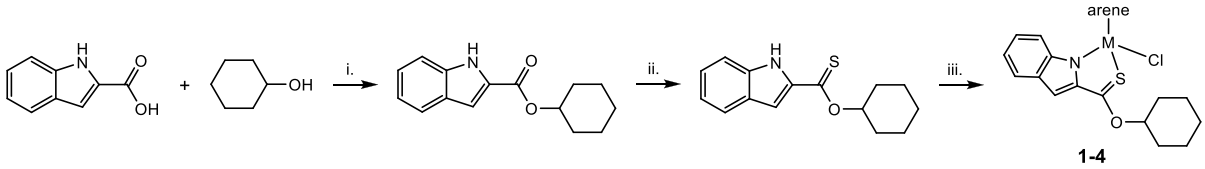

Scheme 1. Synthetic pathway for complexes **1–4**; i) sulfuric acid, cyclohexanol, reflux, 2 h; ii) Lawesson's reagent, toluene, reflux, 4 days; iii) metal dimer, dry triethylamine, dry CH_2Cl_2, RT, 12 h.

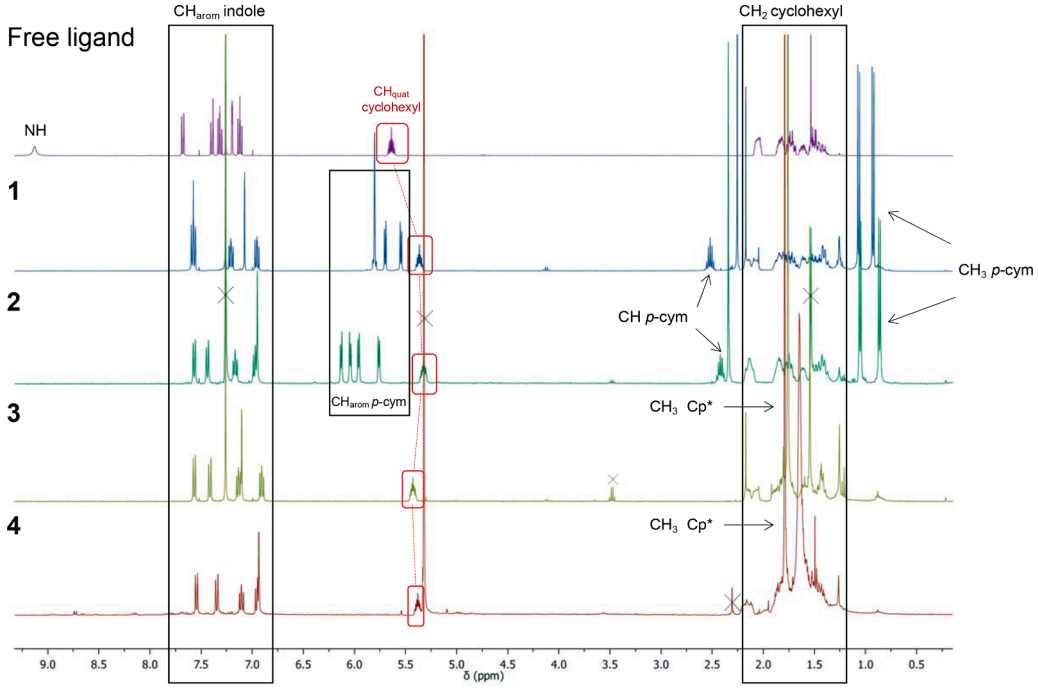

Fig. 3. ^{1}H NMR spectra of free ligand [cyclohexyl indole-2-thionoester] (top), and complexes **1** – **3** below in $CDCl_3$, and **4** in CD_2Cl_2 (400 MHz). Residual solvents are marked with a cross.

The stability and the hydrolysis of complexes **1** – **4** in a mixture of DMSO/RPMI (1:1 v/v) was studied by UV–Vis spectroscopy at 298 K, with spectra being recorded over a period of 24 h (Figure S11). As previously seen for complex **1** [26], 18-electron complexes bearing a chloride ligand undergo an exchange of the halide group for a molecule of water, which allows the determination of their hydrolysis rate ($K_{aquation}$) by plotting the absorbance at a fixed wavelength *versus* time for all compounds (Table 1). A relationship between the anticancer activity and the aquation of the monodentate ligand (X) of certain organoruthenium complexes has been previously established [34–36]. This correlation is important as this aquation is considered to be an activation step which allows further interactions of these half-sandwich complexes with other biomolecules of interest [37–39]. For complexes **1** – **4** the hydrolysis rate depends on the nature of the central metal. Complexes containing a metal from group 8 (ruthenium, osmium) seem to hydrolyse faster than their heavier congeners of group 9 (rhodium, iridium).

Table 1
Reactivity of complexes **1** – **4**. p*K*a values measured using UV–Vis spectroscopy (10^{-5} M, 298 K), in acetonitrile/water (6:94 v/v). Aquation constants and rates of hydrolysis are measured using UV–Vis spectroscopy (10^{-5} M, 298 K), in DMSO/RPMI (1:1 v/v). Log *P* values determined using octanol and water.

Compound	Metal	p*K*a	$K_{aquation}$ (s^{-1})	TOF[a] (h^{-1})	TOF[b] (h^{-1})	Log *P*[c]
1	Ru	9.81 ± 0.07	$1.2 \times 10^{-4} \pm 0.3 \times 10^{-4}$	14.8 ± 0.1	13.9 ± 0.4	5.3
2	Os	10.30 ± 0.02	$1.1 \times 10^{-4} \pm 0.2 \times 10^{-4}$	5.3 ± 0.1	5.4 ± 0.2	5.2
3	Rh	–	$0.9 \times 10^{-4} \pm 0.08 \times 10^{-4}$	9.3 ± 0.5	9.6 ± 0.5	5.3
4	Ir	10.4 ± 0.10	$0.5 \times 10^{-4} \pm 0.05 \times 10^{-4}$	7.2 ± 0.6	7.4 ± 0.5	5.1

[a] Turnover frequencies values measured using UV–Vis spectroscopy (10^{-5} M, 298 K); [b] turnover frequencies values measured using NMR spectroscopy (10^{-4} M, 298 K); [c] Log *P* values experimentally determined using the shake-flask method.

The p*K*a values of the aqua adducts derived from complexes **1** – **4** could be determined by mixing the compounds (previously dissolved in acetonitrile) with different aqueous solutions at known pH ranging from 8 to 12. The p*K*a values (Table 1) were calculated by plotting the absorbance at the corresponding wavelength against the pH and fitting it to the Boltzmann equation to obtain the inflection point (Figure S12). The aqua adducts of complexes **2** and **4** display p*K*a values in the same range as for the aqua adduct of complex **1** and ruthenium complexes bearing similar *N,S*-coordinated indole derivatives [26]. The p*K*a of the aqua adduct of compound **3** could not be determined because of the overlap of absorbance of the aqua- and the hydroxo- compounds [33]. Consequently, at physiological pH of normal cells (7.4) or cancer cells (6.7 – 7.1), only the aqua adduct of the metal complex will be present in solution, which allows further possible interactions with biomolecules such as nucleobases.

The UV–Vis absorption spectra of the four complexes were also recorded in dichloromethane. Strong absorption bands between 350 and 550 nm were observed as expected for all four complexes (see

Figure S13) and arise from ligand-to-metal charge-transfer (LMCT) from the different σ and π orbitals of the heteroatoms to the metal ion, d-d transitions, and metal-to-ligand charge-transfer (MLCT) from M-S and M-N π orbitals to Ru/Os-*p*-cymene or Rh/Ir-Cp* δ* molecular orbitals [40]. The octanol-water partition coefficient (Log *P*) was also determined using the shake-flask method [41], as it provides an indication of the affinity of a molecule for aqueous and lipophilic environments and therefore its ability to cross membranes by passive diffusion [42]. The compounds showed Log *P* values higher than 3, which indicates that they are hydrophobic, as expected (see Table 1, Table S1 and Figure S14). All four values are within the same range, which is not surprising given that the ligands are the same for all four complexes (*p*-cymene and Cp* having a similar hydrophobic character).

2.2. Transfer hydrogenation of NAD^+

Half-sandwich complexes have been applied to many catalytic processes. In the past few years, some of these complexes showed potential as transfer hydrogenation catalysts outside [43] and within cells, being capable of transforming cofactors such as NADH/NAD^+, or affecting in many ways the metabolic routes in cells [17,35,38,44–46]. As previously reported by our group, a family of *N,N*-coordinated indole-based complexes has been shown to be catalytically active as transfer hydrogenation catalysts, unfortunately these results were not reproducible under physiological conditions [33]. Here, to further understand the role of the coordinating heteroatoms on the activity of the carbothiolated indole-containing complexes **1** – **4**, their ability to reduce NAD^+ in presence of an hydride donor such as sodium formate has been studied over time (final concentrations were as follows: complexes **1** - **4** 2.5 mM; NAD^+ 5 mM; $NaHCO_2$ 63 mM; molar ratio 1:2:25). ^{1}H NMR spectra show an increase of the NADH signals over time (Fig. 4 for complex **1**, Figures S15-S17 for complexes **2** – **4**).

The turnover frequencies (TOF) of complexes **1** – **4** were determined both by UV–Vis and NMR spectroscopies in MeOH/H_2O (1:1 v/v) or MeOD/D_2O (1:1 v/v) respectively, at 310 K and pH 7.4 ± 0.2 (Figures S18-S19). As can be seen in Table 1, the reduction of NAD^+ by compounds **1** – **4** is in a range between 5 and 15 h^{-1}, with similar values obtained by both methods, similarly to previously reported compounds containing metals of group 8 and 9 such as ruthenium, osmium, rhodium, and iridium half-sandwich complexes bearing a bidentate ligand [15,31,38,44,47–49].

2.3. Interaction with biomolecules (GSH, nucleobases)

Among all the possible mechanisms of action that metal complexes possess, their binding to biomolecules such as glutathione or nucleobases is one of the most studied [39,50–52]. Additionally, this interaction with sulfur-based biomolecules can be responsible for some side effects and can create mechanisms of resistance [53]. One of the most investigated biomolecules is the tripeptide glutathione which has been studied for its competition to bind metal complexes and prevent their interaction with the desired target such as DNA [54,55]. The binding of complexes **1** – **4** to GSH and nucleobases such as guanine and adenine was therefore studied by ^{1}H NMR spectroscopy at different time points (1 min, 12 and 24 h). The coordination of complexes **1–3** to the sulfur tripeptide glutathione occurred immediately (Fig. 5), yielding 100 % of GSH adducts. The coordination is confirmed by an upfield shift of the resonances accounting for the aromatic protons located on the indole-based ligand. Remarkably, complex **4** did not show any interaction with GSH even after 24 h. This behaviour could be explained by the known relative inertness of iridium complexes towards other ligands [15,56,57].

The ability of complexes **1** – **4** to react with 9-ethylguanine (9-EtG) and 9-methyladenine (9-MetA) was also studied between 0 and 24 h, because DNA is a potential target for metal complexes [36,58–60]. Compounds **1** – **4** were reacted with two molar equivalents of 9-EtG or 9-MetA in aqueous solution at pH 7.4 ± 0.2. Interestingly, all complexes seem to promptly react with 9-EtG (less than 10 min, Fig. 6), but not with 9-MeA (Figure S20) even after 24 h. As seen in Fig. 6, the resonances for the protons of the indole moiety for all complexes change their multiplicity or shift upfield, which demonstrates the fast interaction of these metal complexes with the nucleobase guanine.

This difference of reactivity could be explained by the different affinities of metal complexes towards nucleobases which come from both electronic and steric effects of the purine bases with different central metals [61,62]. Such results demonstrate a more selective behaviour for complexes **1** – **4** compared to platinum drugs which bind to both guanine and adenine [63].

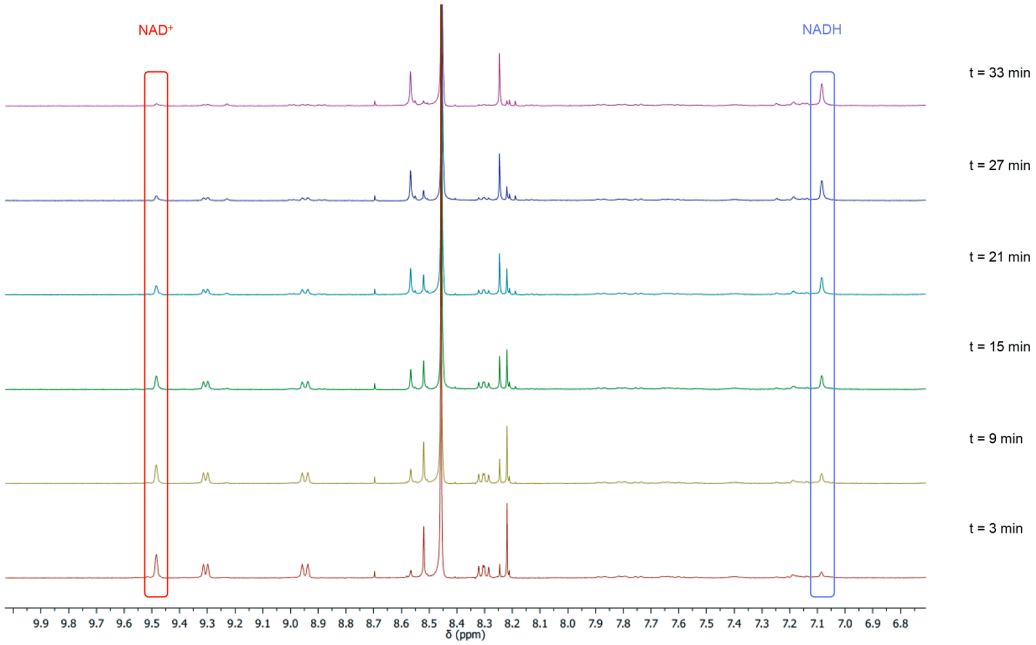

Fig. 4. ^{1}H NMR spectra in $CDCl_3$ (400 MHz) of complex **1** in the presence of NAD^+ and sodium formate (1:2:25) respectively, every 6 min.

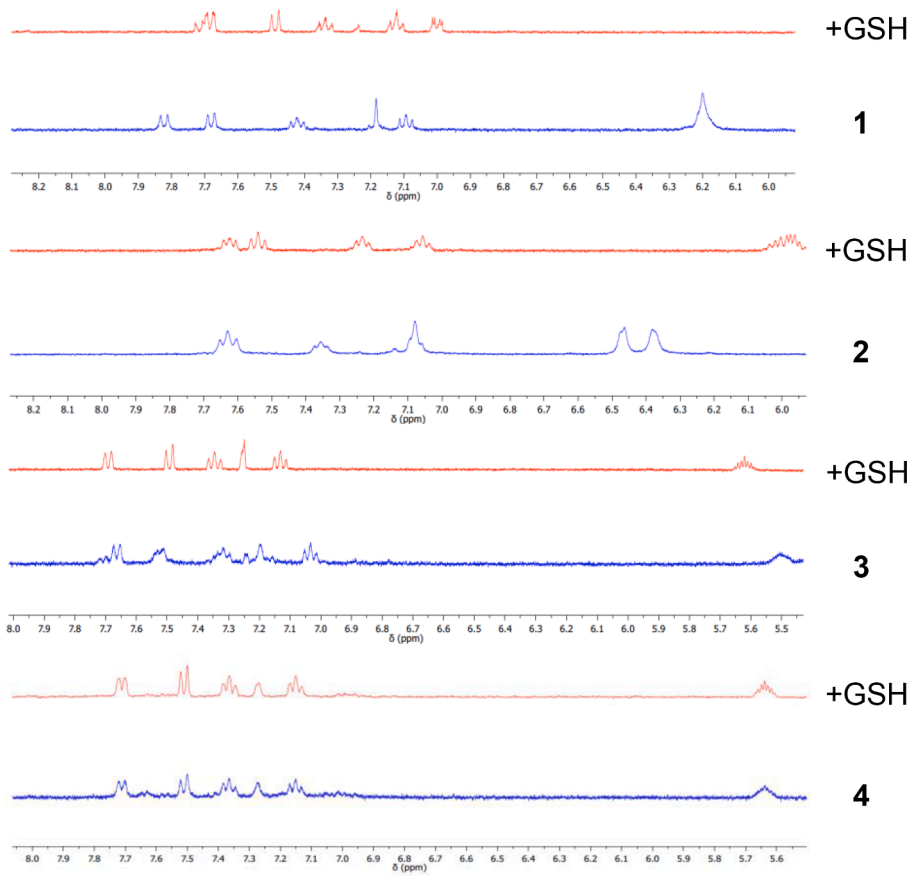

Fig. 5. ^{1}H NMR spectra of complexes **1–4** in the presence of two mol. equiv. of GSH after 24 h (1.1 mM complex, MeOD/D_2O 1:1 v/v, pH 7.4, 298 K).

2.4. Cytotoxicity studies in vitro

The ability of complexes **1** – **4** to induce cell death was evaluated against several cell lines, namely, human ovarian adenocarcinoma (A2780), cisplatin-resistant variant of A2780 (A2780cisR), and normal human prostate epithelial (PNT2). Half-maximal inhibitory concentrations (IC_{50}) were determined using a 24 h MTT assay with 48 h recovery period. The IC_{50} values of compounds **1** – **4** and cisplatin are shown in Table 2. The ligand O-cyclohexyl-*1H*-indole-2-carbothioate is inactive on both cancerous and normal cell lines (IC_{50} > 70 μM) [26].

All complexes showed anticancer activity in the range of cisplatin in A2780 cell line (Figure S21). Interestingly, complexes **1, 2**, and **4** demonstrate little difference in activity against A2780cisR and A2780 cell lines, which could suggest a different MoA from cisplatin. Surprisingly, complex **4** is the only complex of this series, with complex **2** to a lesser extent, that shows no selectivity towards any of the cell lines. The non-binding of this iridium (and osmium) complex towards GSH, the natural detoxifier of the cell, could explain this lack of selectivity as there are increased levels of GSH in A2780cisR cells [64], as well as the known inertness of third-row transition metals compared to second-row equivalents.

Remarkably, from all the complexes, compound **3** is the only one that presents 7x more selectivity towards cancer cells (A2780) than towards normal cells (PNT2), compared to 2–3x more selectivity for the other complexes.

2.5. Cell viability experiments

Sadler et al. have reported some transition metal complexes containing ruthenium, osmium, rhodium, and iridium that catalyse the reduction of the cofactor NAD^+ with formate, an hydride source, within cells [56,65–67]. This is a promising MoA that differs from the already reported DNA binding of cisplatin. Once the complex enters in the mitochondria, it alters the redox homeostasis of the cell, leading to a cell death by an excess of ROS. Encouraged by the promising catalytic properties of the complexes **1** – **4** in a test tube environment (Fig. 4), we investigated their catalytic activity within cells. Initial checks confirmed that formate itself at concentrations from 0 to 2 mM is non-toxic to cells (Fig. 7). Then A2780 cells were co-incubated with equipotent concentrations of complexes **1** – **4** (1/3 × IC_{50}) and different concentration of sodium formate (0, 1, and 2 mM). The antiproliferative activity of complexes **1** – **4** was enhanced by co-administration with formate (Fig. 7). The degree of activity enhancement was directly related to the formate concentration, which is consistent with a direct contribution to the activity from catalytic transfer hydrogenation. The largest decrease in cell survival (around 23 %) was observed for complex **1**, from 69 % to 54 % when the concentration of formate was increased from 0 to 2 mM. These results are in accordance with the TOF values determined under similar conditions (presented in Table 1).

N-acetylcysteine (NAC) is a pro-drug needed to generate L-cysteine inside the organism which is used as a precursor for the synthesis of the known antioxidant GSH [53]. NAC is therefore a known ROS scavenger and can be used to confirm if a MoA of the complexes based on the production of ROS can be hypothesised [68,69]. A2780 cells were co-incubated with NAC at different concentrations (0, 2 and 5 mM) for 30 min before treatment with the complexes at IC_{50} concentrations. Pre-treatment of cells with NAC at high concentrations led to an increase of the cell viability, which indicates that NAC has an inhibitory effect on the cytotoxic activity of complexes **1** – **4**, and can protect cells from the antiproliferative effect of these complexes (Fig. 7).

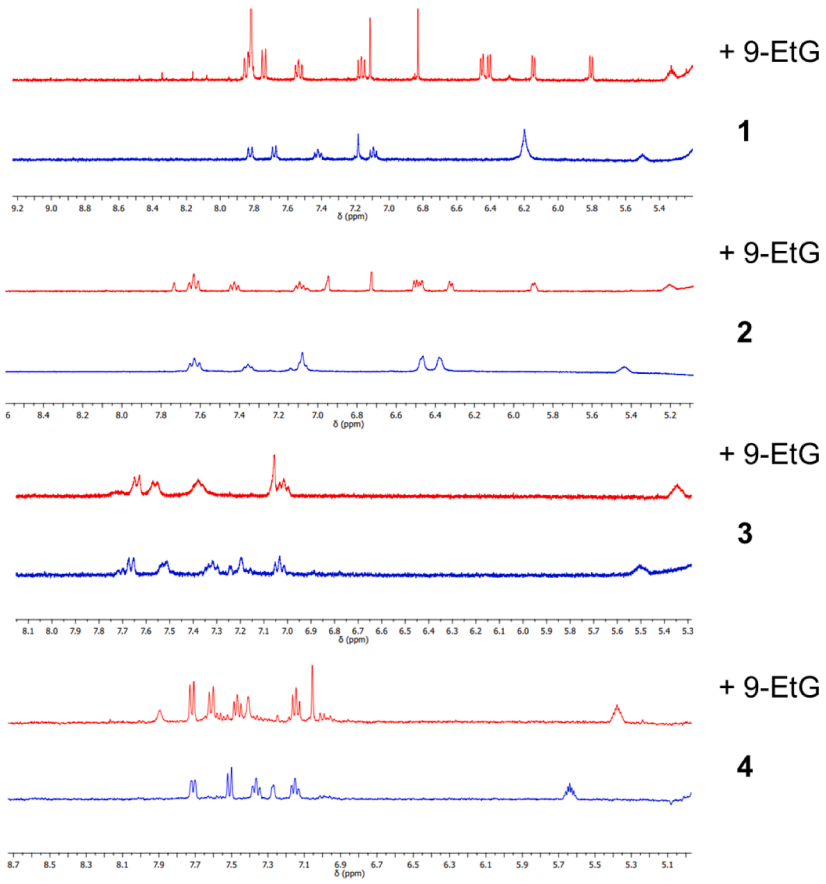

Fig. 6. ^{1}H NMR spectra of complexes **1–4** in the presence of two mol. equiv. of 9-ethylguanine after 24 h (1.1 mM complex, MeOD/D_2O 1:1 v/v, pH 7.4, 298 K).

Table 2
IC_{50} values (μM) in A2780, A2780 cisplatin resistant, MCF7 and PNT2 cells for complexes **1** – **4** ($n = 3$). The selectivity index compares the IC_{50} values for the non-cancer cell line PNT2 to respectively the wild type and cisplatin-resistant ovarian cancer lines.

			IC_{50} values (μM)		Selectivity index	
Compound	Metal	A2780	A2780cisR	PNT2	A2780	A2780cisR
1[a]	Ru	10.7 ± 0.6	15.3 ± 0.9	20.8 ± 0.9	1.94	1.36
2	Os	5.9 ± 0.2	5.0 ± 0.2	5.4 ± 0.5	0.92	1.08
3	Rh	3.2 ± 0.2	9.8 ± 0.8	22.0 ± 1.9	6.86	2.25
4	Ir	3.3 ± 0.3	3.6 ± 0.2	8.4 ± 0.2	2.56	2.35
cisplatin	Pt	5.3 ± 0.5	19.4 ± 1.3	29.2 ± 1.9	5.49	1.51

[a] IC_{50} values taken from ref. [[26]].

2.6. *In vivo studies of complex **1** alone and combination with formate*

Based on the promising *in vitro* results for complex **1** and its association with formate, preclinical studies were progressed *in vivo*. First, the maximum tolerated dose (MTD) for complex **1** was established at 3 mg/kg when administered intraperitoneally (i.p.) daily for four days and monitored for at least 16 days (Figure S22). The MTD for formate was determined at 20 mg/kg (Figure S22).

These efficacy studies are a preliminary study with small groups in order to explore: i) if complex **1** has any activity on its own; ii) if the addition of formate could enhance the potency of complex **1**, and iii) if the combination of complex **1** and formate demonstrates any toxic effects when administered together.

After MTD determination, the efficacy of **1** alone and in combination with formate was studied in A2780 and A2780cisR subcutaneous tumour xenograft models (Table 3 and Figures S23-S24). In the mice-bearing A2780cisR tumours, the highest difference on the tumour growth between both treatments is observed from day 4. Complex **1** alone shows no growth delay, while co-incubation with formate causes some delay in the tumour growth. No toxicity was observed in either study for either compound, as confirmed by the absence of weight loss during the studies (Figures S25-S26). Of importance is the tumour size trend, with the value on day 9 being highly promising in terms of the role of formate, with a lack of effect with complex **1** on its own but with a decrease when formate is co-incubated.

3. Conclusions

In conclusion, four half-sandwich metal complexes (Ru, Os, Rh, and Ir) containing the O-cyclohexyl-*1H*-indole-2-carbothiolate bioactive indole ligand were synthesised and characterised. Following investigation of their stability in solution, *in vitro* screening was performed to gain a first estimation of their cytotoxicity against cancer cells. The complexes were found to be active against A2780 ovarian cancer and A2780cisR cisplatin-resistant ovarian cancer cell lines. Interestingly, the iridium complex **4** shows no difference in the IC_{50} values against all cancerous cell lines and the normal PNT2 cell lines, which suggests no selectivity nor cross-resistance. This could be explained from its inertness towards biomolecules such as glutathione, a natural antioxidant which in living organisms protects cells from the oxidative stress produced by ROS. Differently from complex **4**, complex **3** containing rhodium presents 7x more selectivity towards cancerous cells (A2780) *versus* normal cells (PNT2).

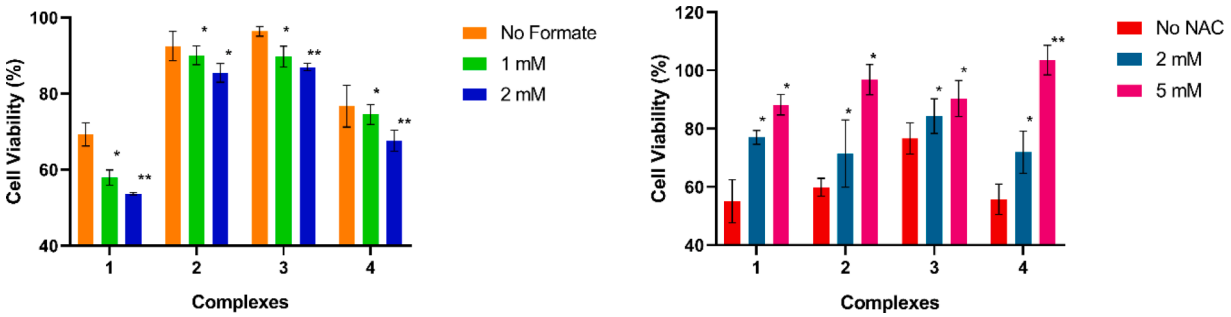

Fig. 7. Cell viability of A2780 cells treated with complexes **1** – **4** in combination with sodium formate (left) or NAC (right). *P*-values were calculated after a *t*-test against the negative control data (without formate or NAC), *$p < 0.05$, **$p < 0.01$.

Table 3
Efficacy of complex **1** associated or not with formate on tumour growth. (RTV = relative tumour volume).

Cell Line	Treatment	Median Time to RTV (days)	Growth Delay (days)	Maximum% Weight Loss
A2780	1	1.8	0.4	1 (day 1)
	1 + formate	2.0	0.6	0
	Control	1.4	–	0
A2780cisR	1	2.6	0.0	0
	1 + formate	4.0	1.2	2 (day 3)
	Control	2.8	–	1 (day 1)

Complexes **1** – **4** were seen to be promising transfer hydrogenation catalysts for the reaction between NAD^+ and sodium formate that acts as a hydride donor, with TOF values in the range 5 – 15 h^{-1}, similar to other previously reported complexes. To correlate the TOF values obtained by NMR spectroscopy with the possible catalytic activity within the cell, exposure of the complexes **1** – **4** and co-incubation with sodium formate was carried out, with the best candidate being the Ru analogue (23 % more toxic towards ovarian cancer cells (A2780) when co-incubated with a nontoxic amount of hydride donor, in this case 2 mM of sodium formate). Furthermore, co-incubation of complexes **1** – **4** and NAC, a ROS scavenger, showed that all complexes might be involved in the production of ROS, more specifically in the redox imbalance of the NAD^+/NADH conversion. These coenzymes play a pivotal role in cell metabolism, and are involved in over 400 cellular reactions within the cell. Because they possess a sensitive equilibrium, modifying such ratios can produce redox stress with can lead to cell death.

Based on the exciting results obtained for this new family of metal complexes, the best catalyst complex, the ruthenium analogue **1**, was moved forward to preliminary preclinical *in vivo* studies in mice. For mice bearing both A2780 and A2780cisR tumours, whilst not statistically significant due to the small sample sizes, a delay in tumour growth was observed in the presence of formate, which contrasts with results obtained for complex **1** alone. Moreover, administering **1** and formate in combination did not result in any visible toxic effects in both studies. These results demonstrate that the presence of sodium formate can enhance the biological activity of **1**, and will thus be incorporated into treatment regimens during further structural optimisation of this lead complex, along with investigation of mechanism of action.

This new strategy, previously reported by Sadler *et al.*, [15] paves the way to more potent anticancer drugs, as sodium formate alone is not toxic toward A2780 and A2780CisR cells, nor *in vivo*. This combination of a toxic metal-based drug and non-toxic co-catalyst provides a new approach for the design of new metal-based anticancer agents. Lower doses of metal complexes could be administered and would provide new mechanisms of action that could be effective against resistant cancers.

4. Materials and methods

4.1. Materials and instrumentations

Hydrated metallic chlorides were purchased from Precious Metals Online. All other chemicals were purchased from Sigma-Aldrich (UK). Non-dried solvents were purchased from Fischer Scientific and used as received. Dichloromethane, tetrahydrofuran, and toluene were dried over molecular sieves (3 Å). All compounds were prepared under a purified dinitrogen atmosphere using standard Schlenk and vacuum line techniques, unless otherwise specified. pH* was adjusted using EDT direction non-glass pocket pH meter with an ISFET silicon chip pH sensor. pH* values (pH readings without correction for the effect of deuterium) of NMR samples were adjusted using KOD solutions in D_2O. ^1H NMR spectra were recorded at 400 MHz, and ^{13}C NMR were recorded at 100 MHz on a Bruker Spectrospin spectrometer using 5 mm NMR tubes. Data processing was carried out using TOPSPIN 4.0.9 (Bruker U.K. Ltd.). Deuterated solvents were purchased from Goss Scientific Instrument. ^1H NMR chemical shifts were internally referenced to the solvent peak: $CHCl_3$ (δ = 7.26 ppm), H_2O (δ = 4.79 ppm), methanol (δ = 3.31 ppm) or DMSO (δ = 2.50 ppm). All UV–Vis spectra were recorded on an Agilent 60 Cary UV–Vis spectrophotometer. All infra-red spectra were recorded on a PerkinElmer Frontier FT-IR spectrometer using attenuated total reflection (ATR). Metal dimers $[(arene)MCl_2]_2$ were synthesised using an Anton Paar microwave synthesis reactor (Monowave 300) and a 20 mL microwave vial equipped with a magnetic stirring bar [70]. Roswell Park Memorial Institute (RPMI) 1640 medium, foetal bovine serum (FBS), penicillin and streptomycin, phosphate-buffered saline (PBS, pH = 7.4), and other tissue culture reagents were purchased from Gibco (Thermo Fisher Scientific, UK). Cell lines were provided by the Institute of Cancer Therapeutics, University of Bradford. Cells were incubated in a ThermoScientific HERAcell 150 incubator and observed under a Nikon ECLIPSE TS100 Microscope.

Complex **1** and the ligand [cyclohexyl indole-2-thionoester] have been previously reported by the group, and their syntheses are performed as in the literature procedure [[26].

4.2. Synthesis and characterisation

[(*p*-cym)RuCl(cyclohexyl indole-2-thionoester)] (1). Complex 1 was prepared following the literature procedure [26]. Briefly, complex **1** was prepared by stirring the dichloro(*p*-cym)ruthenium dimer (70 mg, 0.11 mmol) with the [cyclohexyl indole-2-thionoester] ligand (46 mg, 0.24 mmol) in 15 mL of dry dichloromethane at ambient temperature overnight and in presence of triethylamine (0.46 mmol). The crude product was extracted with an aqueous solution of 0.1 M HCl (3 × 10 mL) and then dried over $MgSO_4$ and filtered. The product was purified by column chromatography (ethyl acetate/hexane 60:40 (v/v)) and recrystallised in dichloromethane/hexane to obtain a bright red solid (30 mg, 58 %).

[(*p*-cym)OsCl(cyclohexyl indole-2-thionoester)] (2). Complex **2** was synthesised following the procedure of complex **1** for 2 h with the [cyclohexyl indole-2-thionoester] ligand (17.9 mg, 0.07 mmol) and the dichloro(*p*-cym)osmium dimer (26 mg, 0.03 mmol). The pure compound **2** was obtained as a dark red solid (17.2 mg, 85 %).

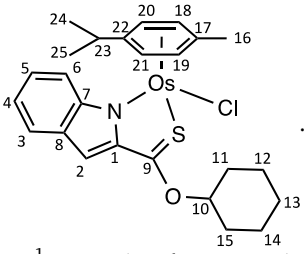

^{1}H NMR ($CDCl_3$, 400 MHz): δ = 7.57 (1H, d, $^3J_{H-H}$ = 8.3 Hz, H6), 7.44 (1H, d, $^3J_{H-H}$ = 8.6 Hz, H3), 7.17 (1H, t, $^3J_{H-H}$ = 7.9 Hz, H4), 6.98 (1H, d, $^3J_{H-H}$ = 7.6 Hz, H5), 6.95 (1H, s, H2), 6.13 (1H, d, $^3J_{H-H}$ = 5.6 Hz, CH *p*-cym), 6.04 (1H, d, $^3J_{H-H}$ = 5.6 Hz, CH *p*-cym), 5.96 (1H, d, $^3J_{H-H}$ = 5.6 Hz, CH *p*-cym), 5.76 (1H, d, $^3J_{H-H}$ = 5.6 Hz, CH *p*-cym), 5.32 (1H, m, H10), 2.42 (1H, sept, $^3J_{H-H}$ = 6.8 Hz, H23), 2.34 (3H, s, H16), 2.20 – 1.36 (10H, br, $H_{cyclohexane}$), 1.05 (3H, d, $^3J_{H-H}$ = 6.9 Hz, H24 or H25), 0.86 ppm (3H, d, $^3J_{H-H}$ = 6.9 Hz, H24 or H25).

$^{13}C\{^1H\}$ NMR ($CDCl_3$, 101 MHz): δ = 214.2 (C9), 151.4 (C1), 144.0 (C7 or C8), 130.2 (C7 or C8), 125.6 (C4), 124.5 (C6), 119.9 (C5), 116.7 (C3), 108.5 (C2), 96.5 (C22), 92.7 (C17), 83.3 (C10), 77.7 ($C_{p\text{-cym}}$), 74.4 ($C_{p\text{-cym}}$), 73.9 ($C_{p\text{-cym}}$), 71.9 ($C_{p\text{-cym}}$), 31.5 (C23), 25.3 ($CH_{2cyclohex.}$), 23.8 ($2CH_{2cyclohex.}$), 23.7 ($2CH_{2cyclohex.}$) 23.4 (C24 or C25), 22.1 (C24 or C25), 18.8 ppm (C16).

IR (ATR) ν_{max}: 3058, 2945, 2925, 2850, 1515, 1259, 779 cm^{-1}.

HRMS (ESI+): *m/z* calc. for $C_{25}H_{30}NOOsS$ [M - Cl]$^+$ 584.1663; found 584.1646.

[(Cp*)RhCl(cyclohexyl indole-2-thionoester)] (3). Complex **3** was synthesised following the procedure of complex **2** with 26.4 mg (0.1 mmol) of ligand and 30 mg (0.05 mmol) of dichloro(Cp*)rhodium dimer. The pure compound **3** was obtained as a bright orange solid (16.4 mg, 64 %).

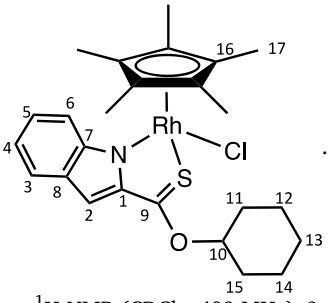

^{1}H NMR ($CDCl_3$, 400 MHz): δ = 7.57 (1H, d, $^3J_{H-H}$ = 8.3 Hz, H6), 7.41 (1H, d, $^3J_{H-H}$ = 8.6 Hz, H3), 7.13 (1H, t, $^3J_{H-H}$ = 7.6 Hz, H4), 7.10 (1H, s, H2), 6.90 (1H, t, $^3J_{H-H}$ = 7.6 Hz, H5), 5.43 (1H, m, H10), 2.20 – 1.35 (10H, br, $H_{cyclohexane}$), 1.76 ppm (15H, s, H17).

$^{13}C\{^1H\}$ NMR ($CDCl_3$, 101 MHz): δ = 204.1 (C9), 149.6 (C1), 146.3 (C7 or C8), 131.1 (C7 or C8), 124.7 (C6), 124.5 (C4), 119.9 (C5), 117.1 (C3), 108.3 (C2), 96.0 (C16), 95.9 (C16), 82.9 (C10), 31.6 ($CH_{2cyclohex.}$), 31.4 ($CH_{2cyclohex.}$), 25.4 ($CH_{2cyclohex.}$), 23.7 ($CH_{2cyclohex.}$), 23.5 ($CH_{2cyclohex.}$), 9.7 ppm (C17).

IR (ATR) ν_{max}: 3043, 2922, 2851, 1512, 1260, 791 cm^{-1}.

HRMS (ESI+): *m/z* calc. for $C_{25}H_{31}NORhS$ [M - Cl]$^+$ 496.1181; found 496.1183.

[(Cp*)IrCl(cyclohexyl indole-2-thionoester)] (4). Complex **4** was synthesised following the procedure of complex **2** with 20.5 mg (0.08 mmol) of ligand and 30 mg (0.04 mmol) of dichloro(Cp*)iridium dimer. The pure compound **4** was obtained as a dark orange solid (14.3 mg, 58 %).

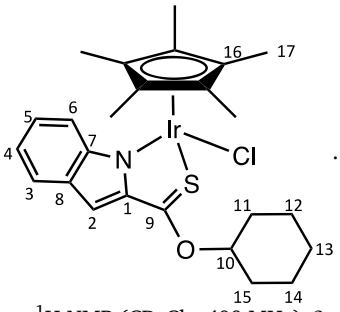

^{1}H NMR (CD_2Cl_2, 400 MHz): δ = 7.54 (1H, d, $^3J_{H-H}$ = 8.4 Hz, H6), 7.35 (1H, d, $^3J_{H-H}$ = 8.6 Hz, H3), 7.11 (1H, t, $^3J_{H-H}$ = 7.8 Hz, H4), 6.95 (1H, t, $^3J_{H-H}$ = 7.4 Hz, H5), 6.94 (1H, s, H2), 5.38 (1H, m, H10), 2.23 – 1.36 (10H, br, $H_{cyclohexane}$), 1.79 ppm (15H, s, H17).

$^{13}C\{^1H\}$ NMR (CD_2Cl_2, 101 MHz): δ = 206.8 (C9), 149.1 (C1), 140.8 (C7 or C8), 130.2 (C7 or C8), 125.2 (C6), 124.8 (C4), 119.9 (C5), 116.7 (C3), 108.4 (C2), 89.2 (C16), 84.07 (C10), 31.9 ($CH_{2cyclohex.}$), 31.8 ($CH_{2cyclohex.}$), 25.8 ($CH_{2cyclohex.}$), 24.2 ($CH_{2cyclohex.}$), 24.1 ($CH_{2cyclohex.}$), 9.8 ppm (C17).

IR (ATR) ν_{max}: 3037, 2939, 2925, 2860, 1516, 1270, 956, 758 cm^{-1}.

HRMS (ESI+): *m/z* calc. for $C_{25}H_{31}NOIrS$ [M - Cl]$^+$ 586.1756; found 586.1759.

4.3. Solution chemistry

Stability determination: Complexes **1** – **4** were dissolved in MeOD (2.2 mM) and diluted to a final concentration of 1.1 mM with either MeOD or D_2O. ^{1}H NMR spectra were recorded at $t \leq 10$ min, 12 h and 24 h. p*K*a determination: Complexes **1** – **4** were dissolved in acetonitrile/H_2O 6:94 (v/v) and UV-Vis spectra of the samples were recorded increasing the pH from 7 to 12, using a 0.1 M solution of NaOH. p*K*a value of each complex was determined by plotting the absorbance against the pH. Hydrolysis rate: Complexes **1** – **4** were dissolved in DMSO/RPMI 1:1 (v/v) (3×10^{-5} M) at room temperature and UV-Vis spectra of the samples were recorded every four minutes between $t \leq$ 10 min and 24 h. The dissociation constant values were calculated by plotting the absorbance against the time at fixed wavelength.

The log *P* values were determined using the shake-flask method. 2 mL of octanol were pre-saturated with 2 mL of phosphate-buffered saline (PBS) by overnight incubation with shaking of a biphasic mixture of the two at room temperature. 5 μL of a 10 mM DMSO stock solution of each compound was added into the biphasic solution of PBS/octanol to give a final concentration around 50–100 μM. The mixture was shaken for several hours and allowed to stand for 2 h. Aliquots from the octanol phase and the aqueous phase were extracted and analysed by UV–Vis spectroscopy to determine their relative concentrations in each phase.

4.4. NAD^+ reduction

Transfer hydrogenation reactions with complexes **1** – **4** (catalyst), sodium formate, and NAD^+ were studied by mixing a solution of the corresponding complex (3.2 mM, MeOD), sodium formate (348 mM, D_2O) and NAD^+ (15 mM, D_2O). Final concentrations of 2.5 mM for the complex, 5 mM for NAD^+ and 62.5 mM for $NaHCO_2$ were obtained (molar ratio 1:2:25). The pH of the mixture was adjusted to 7.4 ± 0.2. ^{1}HNMR spectra were recorded at 310 K every 3 min until completion of the reaction. Molar ratios of NAD^+ and NADH were determined by integrating the area under the signals associated with NAD^+ (9.33 ppm) and 1,4-NADH (6.96 ppm). The turnover number (TON) for the reaction was calculated as follows:

$$TON = \frac{I_{6.96}}{I_{6.96} + I_{9.33}} \frac{[NAD]_0}{[catalyst]}$$

where I_n is the integral of the signal at n ppm and $[NAD^+]_0$ is the concentration of NAD^+ at the start of the reaction.

4.5. Interaction with biomolecules (GSH, nucleobases)

The reactions of complexes **1** – **4** with glutathione (GSH), 9-ethylguanine (9-EtG) and 9-methyladenine (9-MetA) were studied. MeOD solutions of complexes **1** – **4** (2.2 mM) were mixed with a solution of the corresponding nucleobase in D_2O (4.4 mM) and the pH adjusted to 7.4 ± 0.2. Final concentrations of 1.1 mM for the complex and 2.2 mM for glutathione/nucleobase were obtained. ^{1}H NMR spectra of the resulting mixture were recorded at $t \leq 10$ min and 24 h in MeOD/D_2O (1:1 v/v).

4.6. Cytotoxicity studies in vitro

In vitro chemosensitivity tests were performed against A2780, A2780cisR, and PNT2 cells. Cancer cell lines were routinely maintained as monolayer cultures in RPMI medium supplemented with 10 % foetal calf serum, penicillin (100 I.U./mL), streptomycin (100 μg/mL), sodium pyruvate (1 mM), and L-glutamine (2 mM). For chemosensitivity studies, cells were incubated in 96-well plates at a concentration of 7.5×10 [3] cells per well and the plates were incubated for 24 h at 37 °C and a 5 % CO_2-humidified atmosphere prior to drug exposure. Complexes were dissolved in DMSO to provide stock solutions which were further diluted with media to provide a range of final concentrations. Drug-media solutions were added to cells (the final concentration of DMSO was less than 1 % (v/v) in all cases) and incubated for 24 h at 37 °C and 5 % CO_2-humidified atmosphere. The drug-media was removed from the wells and the cells were washed with PBS (100 μL, twice), and 100 μL of complete fresh media were added to each well. The plates were further incubated for 48 h at 37 °C in a 5 % CO_2-humidified atmosphere to allow for a period of recovery. 3-(4,5-dimethylthiazol-2-yl)−2,5-diphenyltetrazolium bromide (MTT) (20 μL, 2.5 mg/mL) was added to each well and incubated for 2 h at 37 °C and 5 % CO_2-humidified atmosphere. All solutions were then removed and 100 μL of DMSO was added to each well in order to dissolve the purple formazan crystals. A Thermo Scientific Multiskan EX microplate photometer was used to measure the absorbance in each well at 570 nm. Cell survival was determined as the absorbance of treated cells divided by the absorbance of controls and expressed as a percentage. The IC_{50} values were determined from plots of % survival against drug concentration. Each experiment was repeated in triplicates of triplicates and a mean value was obtained and stated as IC_{50} (μM) ± SD. Cisplatin was also used as a positive control.

4.7. Cell viability experiments

Cells were incubated in 96-well plates at a concentration of 7.5×10^3 cells per well and the plates were incubated for 24 h at 37 °C and a 5 % CO_2-humidified atmosphere prior to drug exposure. Complexes were dissolved in DMSO to provide stock solutions, which were further diluted with media to working concentrations. Solutions of *N*-acetylcysteine (NAC) or sodium formate in media were also prepared. Drug-media solutions and NAC or sodium formate solutions were added to cells (final concentrations as follows: IC_{50} values for the complex for NAC experiment and $1/3 \times IC_{50}$ for co-incubation with sodium formate; 0, 2, and 5 mM for NAC; 0, 1, and 2 mM for sodium formate; DMSO concentration was less than 1 % (v/v) in all cases) and incubated for 24 h at 37 °C in a 5 % CO_2-humidified atmosphere. After 24 h of incubation, the drug-media was removed from the wells and the cells were washed with PBS (100 μL, twice), and 100 μL of fresh media were added to each well. The plates were further incubated for 48 h at 37 °C in a 5 % CO_2-humidified atmosphere to allow for a period of recovery. 3-(4,5-dimethylthiazol-2-yl)−2,5-diphenyltetrazolium bromide (MTT) (20 μL, 2.5 mg/mL) was added to each well and incubated for 2 h at 37 °C and 5 % CO_2-humidified atmosphere. All solutions were then removed and 100 μL of DMSO was added to each well in order to dissolve the purple formazan crystals. A Thermo Scientific Multiskan EX microplate photometer was used to measure the absorbance in each well at 570 nm. Cell survival was determined as the absorbance of treated cells divided by the absorbance of controls and expressed as a percentage.

4.8. In vivo studies of complex *1* alone and combination with formate

4.8.1. Compound

All compounds were provided in powdered form and stored in a −20 °C freezer. They were formulated just before use. Complex **1** was firstly dissolved in dimethyl sulfoxide (DMSO) in a volume equal to 10 % of the final concentration, vortexed, and diluted in arachis oil to produce the required dose. Formate was dissolved in PBS to produce the required dose. The drugs were then administered within 10 min of initial dilution.

4.8.2. Animals

Female Balb/c immunodeficient nude mice aged 6–12 weeks were used (Envigo, Blackthorn, UK). Mice were kept in cages housed in isolation cabinets in an air-conditioned room with regular alternating cycles of light and darkness. They received Teklad 2018 diet (Envigo, Blackthorn, UK) and water *ad libitum*. All animal procedures were carried out under a project licence issued by the UK Home Office and UK National Cancer Research Institute Guidelines for the Welfare of Animals were followed throughout.

4.8.3. Evaluation of MTD

The compounds were prepared fresh on the days of treatment as described above and administered i.p. to groups of two mice in a volume of 0.1 mL per 10 g of body weight. The first day of treatment was denoted as Day 0. Compounds were administered to non-tumour-bearing animals on days 0, 1, 2, 3, and 4. A group of two untreated control animals was included in each MTD study. Following treatment, body weight was measured on a regular basis, and behaviour and general appearance monitored visually to assess for deleterious effects (*e.g.*, dehydration, impaired mobility, hunched posture, low body temperature, ulceration and significant body weight loss), with any effects during the study recorded. If body weight loss was >15 % over a 72-hour period or if animal behaviour and appearance were significantly altered, then mice were immediately sacrificed by cervical dislocation. If no deleterious effects were seen after at least 16 days of study, then the animals were sacrificed and the dose considered non-toxic.

4.8.4. S.c. xenograft tumours

A2780/WT and A2780/*cis* tumours were excised from a donor animal, placed in sterile physiological saline containing antibiotics and cut into small fragments of approximately 5 mm^3. Under brief general inhalation anaesthesia, fragments were implanted in the flank of each mouse using a trocar. Once the tumours could accurately be measured by callipers, the mice were allocated into groups (control or treated) by restricted randomisation to keep group mean tumour size variation to a minimum, with three animals set up per group.

4.8.5. Evaluation of efficacy in s.c. xenograft models

The compound was prepared fresh on the days of treatment as described above and administered i.p. to mice on days 0–4 in a volume of 0.1 mL per 10 g of body weight. Complex **1** was administered at 3 mg/kg/dose and one group received compound **1** at 3 mg/kg/dose plus formate at 20 mg/kg/dose. The negative control group was untreated.

The effects of therapy were assessed by frequent monitoring growth of the tumours and body weight. Two-dimensional caliper measurements of the tumours were taken, and volumes calculated using the formula $(a^2 \times b)/2$, where a is the smaller and b the larger diameter of the tumour. Tumour volume was then normalised to the respective volume on Day 0, and semi-log plots of relative tumour volume (RTV) *versus* time were made. Mann-Whitney U tests were performed to determine the statistical significance of any differences in growth rate

(based on tumour volume doubling time, RTV2) between control and treated groups.

CRediT authorship contribution statement

Laia Rafols: Writing – review & editing, Writing – original draft, Methodology, Investigation, Formal analysis. **Maria Azmanova:** Writing – review & editing, Writing – original draft, Methodology, Investigation, Formal analysis. **Nathan Perrigault:** Formal analysis, Methodology. **Patricia A. Cooper:** Methodology, Investigation. **Steven D. Shnyder:** Writing – review & editing, Visualization, Validation, Methodology, Investigation, Formal analysis. **William H.C. Martin:** Writing – review & editing, Supervision, Resources. **Anaïs Pitto-Barry:** Writing – review & editing, Writing – original draft, Visualization, Validation, Supervision, Resources, Project administration, Methodology, Investigation, Funding acquisition, Formal analysis, Data curation, Conceptualization.

Declaration of competing interest

The authors declare that they have no known competing financial interests or personal relationships that could have appeared to influence the work reported in this paper.

Data availability

Data will be made available on request.

Acknowledgements

APB is grateful to Prof. N. P. E. Barry for his support. The support of the Royal Society (University Research Fellowship No. URF150295), the Academy of Medical Sciences/the Wellcome Trust/the Government Department of Business, Energy and Industrial/the British Heart Foundation Springboard Award (SBF003\1170), the CNRS, the Université Paris-Saclay (ANR-20-IDEES-0002), and the CNRS is acknowledged. LRP is supported by a PhD studentship funded by the University of Bradford.

Supplementary materials

Supplementary material associated with this article can be found, in the online version, at doi:10.1016/j.jorganchem.2024.123168.

References

[1] WHO, Fact sheets 2019, https://www.who.int/newsroom/fact-sheets/detail/cancer.
[2] B. Rosenberg, L. Van Camp, T. Krigas, Inhibition of cell division in escherichia coli by electrolysis products from a platinum electrode, Nature 205 (1965) 698–699.
[3] Roberts, J.J.; Thomson, A.J.: The mechanism of action of antitumor platinum compounds. In *Prog. Nucleic Acid Res. Mol. Biol.*; Cohn, W.E., Ed.; Academic Press, 1979; Vol. 22; pp 71–133.
[4] C. Imberti, P.J. Sadler, 150 years of the periodic table: new medicines and diagnostic agents, Adv. Inorg. Chem. 75 (2020) 3–56.
[5] C. Imberti, P. Zhang, H. Huang, P.J. Sadler, New designs for phototherapeutic transition metal complexes, Angew. Chem. Int. Ed. 59 (2020) 61–73.
[6] Y.C. Ong, G. Gasser, Organometallic compounds in drug discovery: past, present and future, Drug Discovery Today: Technol 37 (2020) 117–124.
[7] B.S. Murray, P.J. Dyson, Recent progress in the development of organometallics for the treatment of cancer, Curr. Opin. Chem. Biol. 56 (2020) 28–34.
[8] H. Madec, F. Figueiredo, K. Cariou, S. Roland, M. Sollogoub, G. Gasser, Metal complexes for catalytic and photocatalytic reactions in living cells and organisms, Chem. Sci. 14 (2023) 409–442.
[9] E. Alessio, L. Messori, NAMI-A and KP1019/1339, two iconic ruthenium anticancer drug candidates face-to-face: a case story in medicinal inorganic chemistry, Molecules 24 (2019) 1995.
[10] S. Monro, K.L. Colón, H. Yin, J. Roque III, P. Konda, S. Gujar, R.P. Thummel, L. Lilge, C.G. Cameron, S.A McFarland, Transition metal complexes and photodynamic therapy from a tumor-centered approach: challenges, opportunities, and highlights from the development of TLD1433, Chem. Rev. 119 (2019) 797–828.
[11] M.S. Sanford, J.A. Love, R.H. Grubbs, Mechanism and activity of ruthenium olefin metathesis catalysts, J. Am. Chem. Soc. 123 (2001) 6543–6554.
[12] G.C. Vougioukalakis, R.H. Grubbs, Ruthenium-based heterocyclic carbene-coordinated olefin metathesis catalysts, Chem. Rev. 110 (2010) 1746–1787.
[13] A.L. Noffke, A. Habtemariam, A.M. Pizarro, P.J. Sadler, Designing organometallic compounds for catalysis and therapy, Chem. Commun. 48 (2012) 5219–5246.
[14] J.J. Soldevila-Barreda, P.J. Sadler, Approaches to the design of catalytic metallodrugs, Curr. Opin. Chem. Biol. 25 (2015) 172–183.
[15] J.J. Soldevila-Barreda, I. Romero-Canelón, A. Habtemariam, P.J. Sadler, Transfer hydrogenation catalysis in cells as a new approach to anticancer drug design, Nat. Commun. 6 (2015) 6582.
[16] H. Huang, S. Banerjee, K. Qiu, P. Zhang, O. Blacque, T. Malcomson, M.J. Paterson, G.J. Clarkson, M. Staniforth, V.G. Stavros, G. Gasser, H. Chao, P.J. Sadler, Targeted photoredox catalysis in cancer cells, Nat. Chem. 11 (2019) 1041–1048.
[17] S. Banerjee, P.J. Sadler, Transfer hydrogenation catalysis in cells, RSC Chem. Biol. 2 (2021) 12–29.
[18] R.E. Morris, R.E. Aird, P. del Socorro Murdoch, H. Chen, J. Cummings, N. D. Hughes, S. Parsons, A. Parkin, G. Boyd, D.I. Jodrell, P.J Sadler, Inhibition of cancer cell growth by ruthenium(II) arene complexes, J. Med. Chem. 44 (2001) 3616–3621.
[19] S.J. Dougan, P.J. Sadler, The design of organometallic ruthenium arene anticancer agents, Chimia 61 (2007) 704–715.
[20] A. Bergamo, A. Masi, A.F.A. Peacock, A. Habtemariam, P.J. Sadler, G. Sava, *In vivo* tumour and metastasis reduction and *in vitro* effects on invasion assays of the ruthenium RM175 and osmium AFAP51 organometallics in the mammary cancer model, J. Inorg. Biochem. 104 (2010) 79–86.
[21] J.J. Soldevila-Barreda, P.C.A. Bruijnincx, A. Habtemariam, G.J. Clarkson, R. J. Deeth, P.J. Sadler, Improved catalytic activity of ruthenium–arene complexes in the reduction of NAD+, Organometallics 31 (2012) 5958–5967.
[22] F. Chen, J.J. Soldevila-Barreda, I. Romero-Canelon, J.P.C. Coverdale, J.-I. Song, G. J. Clarkson, J. Kasparkova, A. Habtemariam, V. Brabec, J.A. Wolny, V. Schunemann, P.J. Sadler, Effect of sulfonamidoethylenediamine substituents in RuII arene anticancer catalysts on transfer hydrogenation of coenzyme NAD+ by formate, Dalton Trans. 47 (2018) 7178–7189.
[23] R.E. Aird, J. Cummings, A.A. Ritchie, M. Muir, R.E. Morris, H. Chen, P.J. Sadler, D. I. Jodrell, *In vitro* and *in vivo* activity and cross resistance profiles of novel ruthenium (II) organometallic arene complexes in human ovarian cancer, Br. J. Cancer 86 (2002) 1652–1657.
[24] S.J. Dougan, A. Habtemariam, S.E. McHale, S. Parsons, P.J. Sadler, Catalytic organometallic anticancer complexes, Proc. Natl. Acad. Sci. 105 (2008) 11628.
[25] W.-Y. Zhang, S. Banerjee, G.M. Hughes, H.E. Bridgewater, J.-I. Song, B.G. Breeze, G.J. Clarkson, J.P.C. Coverdale, C. Sanchez-Cano, F. Ponte, E. Sicilia, P.J. Sadler, Ligand-centred redox activation of inert organoiridium anticancer catalysts, Chem. Sci. 11 (2020) 5466–5480.
[26] V.C. Nolan, L. Rafols, J. Harrison, J.J. Soldevila-Barreda, M. Crosatti, N.J. Garton, M. Wegrzyn, D.L. Timms, C.C. Seaton, H. Sendron, M. Azmanova, N.P.E. Barry, A. Pitto-Barry, J.A.G Cox, Indole-containing arene-ruthenium complexes with broad spectrum activity against antibiotic-resistant bacteria, Curr. Res. Microb. Sci. 3 (2022) 100099.
[27] B.J. Bloomer, D.S. Clark, J.F. Hartwig, Progress, challenges, and opportunities with artificial metalloenzymes in biosynthesis, Biochemistry 62 (2023) 221–228.
[28] A.D. Liang, J. Serrano-Plana, R.L. Peterson, T.R. Ward, Artificial metalloenzymes based on the biotin–streptavidin technology: enzymatic cascades and directed evolution, Acc. Chem. Res. 52 (2019) 585–595.
[29] R. Ramos, J.M. Zimbron, S. Thorimbert, L.-M. Chamoreau, A. Munier, C. Botuha, A. Karaiskou, M. Salmain, J. Sobczak-Thépot, Insights into the antiproliferative mechanism of (C^N)-chelated half-sandwich iridium complexes, Dalton Trans. 49 (2020) 17635–17641.
[30] A.H. Ngo, L.H. Do, Structure–activity relationship study of half-sandwich metal complexes in aqueous transfer hydrogenation catalysis, Inorg. Chem. Front. 7 (2020) 583–591.
[31] K. Tyagi, T. Dixit, V. Venkatesh, Recent advances in catalytic anticancer drugs: mechanistic investigations and future prospects, Inorg. Chim. Acta 533 (2022) 120754.
[32] J. Zhang, A. Pitto-Barry, L. Shang, N.P.E Barry, Anti-inflammatory activity of electron-deficient organometallics, R. Soc. Open Sci. 4 (2017) 170786.
[33] J.J. Soldevila-Barreda, K.B. Fawibe, M. Azmanova, L. Rafols, A. Pitto-Barry, U. B. Eke, N.P.E.Synthesis Barry, Characterisation and In vitro anticancer activity of catalytically active indole-based half-sandwich complexes, Molecules 25 (2020) 4540.
[34] M. Bacac, A.C.G. Hotze, K.v.d. Schilden, J.G. Haasnoot, S. Pacor, E. Alessio, G. Sava, J. Reedijk, The hydrolysis of the anti-cancer ruthenium complex NAMI-A affects its DNA binding and antimetastatic activity: an NMR evaluation, J. Inorg. Biochem. 98 (2004) 402–412.
[35] Z. Liu, I. Romero-Canelón, B. Qamar, J.M. Hearn, A. Habtemariam, N.P.E. Barry, A. M. Pizarro, G.J. Clarkson, P.J. Sadler, The potent oxidant anticancer activity of organoiridium catalysts, Angew. Chem. Int. Ed. 53 (2014) 3941–3946.
[36] R.J. Needham, C. Sanchez-Cano, X. Zhang, I. Romero-Canelón, A. Habtemariam, M.S. Cooper, L. Meszaros, G.J. Clarkson, P.J. Blower, P.J. Sadler, In-cell activation of organo-osmium(II) anticancer complexes, Angew. Chem. Int. Ed. 56 (2017) 1017–1020.
[37] I. Berger, M. Hanif, A. Nazarov Alexey, G. Hartinger Christian, O. John Roland, L. Kuznetsov Maxim, M. Groessl, F. Schmitt, O. Zava, F. Biba, B. Arion Vladimir, M. Galanski, A. Jakupec Michael, L. Juillerat-Jeanneret, J. Dyson Paul, K. Keppler Bernhard, In Vitro anticancer activity and biologically relevant metabolization of

organometallic ruthenium complexes with carbohydrate-based ligands, Chem. Eur. J. 14 (2008) 9046–9057.
[38] J.J. Soldevila-Barreda, A. Habtemariam, I. Romero-Canelón, P.J. Sadler, Half-sandwich rhodium(III) transfer hydrogenation catalysts: reduction of NAD+ and pyruvate, and antiproliferative activity, J. Inorg. Biochem. 153 (2015) 322–333.
[39] X. Zhang, F. Ponte, E. Borfecchia, A. Martini, C. Sanchez-Cano, E. Sicilia, P. J. Sadler, Glutathione activation of an organometallic half-sandwich anticancer drug candidate by ligand attack, Chem. Commun. 55 (2019) 14602–14605.
[40] A. Pitto-Barry, A. Lupan, M. Zegke, T. Swift, A.A.A. Attia, R.M. Lord, N.P.E Barry, Pseudo electron-deficient organometallics: limited reactivity towards electron-donating ligands, Dalton Trans. 46 (2017) 15676–15683.
[41] S.K. Poole, C.F. Poole, Separation methods for estimating octanol–water partition coefficients, J. Chromatogr. B 797 (2003) 3–19.
[42] X. Liu, B. Testa, A. Fahr, Lipophilicity and its relationship with passive drug permeation, Pharm. Res. 28 (2011) 962–977.
[43] U. Işık, N. Meriç, C. Kayan, A. Kılıç, Y. Belyankova, A. Zazybin, M. Aydemir, Synthesis of half-sandwich ruthenium(II) and iridium(III) complexes containing imidazole-based phosphinite ligands and their use in catalytic transfer hydrogenation of acetophenone with isopropanol, J. Organomet. Chem. 998 (2023) 122800.
[44] Z. Liu, R.J. Deeth, J.S. Butler, A. Habtemariam, M.E. Newton, P.J. Sadler, Reduction of quinones by NADH catalyzed by organoiridium complexes, Angew. Chem. Int. Ed. 52 (2013) 4194–4197.
[45] J. Li, Z. Tian, X. Ge, Z. Xu, Y. Feng, Z. Liu, Design, synthesis, and evaluation of fluorine and Naphthyridine–Based half-sandwich organoiridium/ruthenium complexes with bioimaging and anticancer activity, Eur. J. Med. Chem. 163 (2019) 830–839.
[46] S. Infante-Tadeo, V. Rodríguez-Fanjul, A. Habtemariam, A.M. Pizarro, Osmium(ii) tethered half-sandwich complexes: pH-dependent aqueous speciation and transfer hydrogenation in cells, Chem. Sci. 12 (2021) 9287–9297.
[47] L. Yang, S. Bose, A.H. Ngo, L.H. Do, Innocent but deadly: nontoxic organoiridium catalysts promote selective cancer cell death, ChemMedChem 12 (2017) 292–299.
[48] E. Ortega, J.G. Yellol, M. Rothemund, F.J. Ballester, V. Rodríguez, G. Yellol, C. Janiak, R. Schobert, J. Ruiz, A new C,N-cyclometalated osmium(ii) arene anticancer scaffold with a handle for functionalization and antioxidative properties, Chem. Commun. 54 (2018) 11120–11123.
[49] P.K. A, N. Roy, U. Das, S. Varddhan, S.K. Sahoo, P. Paira, [Ru(η6-p-cymene)(N^O 8-hydroxyquinoline)(PTA)] complexes as rising stars in medicinal chemistry: synthesis, properties, biomolecular interactions, *in vitro* anti-tumor activity toward human brain carcinomas, and *in vivo* biodistribution and toxicity in a zebrafish model, Dalton Trans. 51 (2022) 8497–8509.
[50] B.J. Pages, D.L. Ang, E.P. Wright, J.R. Aldrich-Wright, Metal complex interactions with DNA, Dalton. Trans. 44 (2015) 3505–3526.
[51] A. Bergamo, P.J. Dyson, G. Sava, The mechanism of tumour cell death by metal-based anticancer drugs is not only a matter of DNA interactions, Coord. Chem. Rev. 360 (2018) 17–33.
[52] Pragti, B.K. Kundu, S Mukhopadhyay, Target based chemotherapeutic advancement of ruthenium complexes, Coord. Chem. Rev. 448 (2021) 214169.
[53] R. Franco, J.A. Cidlowski, Apoptosis and glutathione: beyond an antioxidant, Cell Death Differ. 16 (2009) 1303–1314.
[54] M. Kartalou, J.M. Essigmann, Mechanisms of resistance to cisplatin, Mutat. Res. 478 (2001) 23–43.
[55] F. Wang, J. Xu, K. Wu, S.K. Weidt, C.L. Mackay, P.R.R. Langridge-Smith, P. J. Sadler, Competition between glutathione and DNA oligonucleotides for ruthenium(ii) arene anticancer complexes, Dalton Trans. 42 (2013) 3188–3195.
[56] Z. Liu, P.J. Sadler, Organoiridium complexes: anticancer agents and catalysts, Acc. Chem. Res. 47 (2014) 1174–1185.
[57] J. Yang, H.-J. Fang, Q. Cao, Z.-W. Mao, The design of cyclometalated iridium(iii)–metformin complexes for hypoxic cancer treatment, Chem. Commun. 57 (2021) 1093–1096.
[58] J. Kasparkova, V. Brabec, Ruthenium coordination compounds of biological and biomedical significance. DNA binding agents, Coord. Chem. Rev. 376 (2018) 75–94.
[59] S.Cisplatin Ghosh, The first metal based anticancer drug, Bioorg. Chem. 88 (2019) 102925.
[60] L.A. Hager, S. Mokesch, C. Kieler, S. Alonso-de Castro, D. Baier, A. Roller, W. Kandioller, B.K. Keppler, W. Berger, L. Salassa, A. Terenzi, Ruthenium–arene complexes bearing naphthyl-substituted 1,3-dioxoindan-2-carboxamides ligands for G-quadruplex DNA recognition, Dalton Trans. 48 (2019) 12040–12049.
[61] H. Chen, J.A. Parkinson, S. Parsons, R.A. Coxall, R.O. Gould, P.J. Sadler, Organometallic ruthenium(II) diamine anticancer complexes: arene-nucleobase stacking and stereospecific hydrogen-bonding in guanine adducts, J. Am. Chem. Soc. 124 (2002) 3064–3082.
[62] A.F.A. Peacock, M. Melchart, R.J. Deeth, A. Habtemariam, S. Parsons, P.J. Sadler, Osmium(II) and ruthenium(II) arene maltolato complexes: rapid hydrolysis and nucleobase binding, Chem. - Eur. J. 13 (2007) 2601–2613.
[63] M.-H. Baik, R.A. Friesner, S.J. Lippard, Theoretical study of cisplatin binding to purine bases: why does cisplatin prefer guanine over adenine? J. Am. Chem. Soc. 125 (2003) 14082–14092.
[64] S.-H. Chen, J.-Y. Chang, New insights into mechanisms of cisplatin resistance: from tumor cell to microenvironment, Int. J. Mol. Sci. 20 (2019) 4136.
[65] S. Betanzos-Lara, Z. Liu, A. Habtemariam, A.M. Pizarro, B. Qamar, P.J. Sadler, Organometallic ruthenium and iridium transfer-hydrogenation catalysts using coenzyme NADH as a cofactor, Angew. Chem. Int. Ed. 51 (2012) 3897–3900.
[66] W.-Y. Zhang, H.E. Bridgewater, S. Banerjee, J.J. Soldevila-Barreda, G.J. Clarkson, H. Shi, C. Imberti, P.J. Sadler, Ligand-controlled reactivity and cytotoxicity of cyclometalated rhodium(III) complexes, Eur. J. Inorg. Chem. (2019) 1052–1060.
[67] E.M. Bolitho, J.P.C. Coverdale, H.E. Bridgewater, G.J. Clarkson, P.D. Quinn, C. Sanchez-Cano, P.J. Sadler, Tracking reactions of asymmetric organo-osmium transfer hydrogenation catalysts in cancer cells, Angew. Chem. Int. Ed. 60 (2021) 6462–6472.
[68] T. Zaidieh, J.R. Smith, K.E. Ball, Q. An, ROS as a novel indicator to predict anticancer drug efficacy, BMC Cancer 19 (2019) 1224.
[69] J. Soldevila-Barreda, M. Azmanova, A. Pitto-Barry, P. Cooper, S. Shnyder, N. Barry, Preclinical anticancer activity of an electron-deficient organoruthenium(II) complex, ChemMedChem 15 (2020) 982–987.
[70] J. Tönnemann, J. Risse, Z. Grote, R. Scopelliti, K. Severin, Efficient and rapid synthesis of Chlorido-bridged half-sandwich complexes of ruthenium, rhodium, and iridium by microwave heating, Eur. J. Inorg. Chem. 2013 (2013) 4558–4562.